ELSEVIER

International Journal of Heat and Fluid Flow 21 (2000) 176–185

International Journal of HEAT AND FLUID FLOW

www.elsevier.com/locate/ijhff

Chaotic fluid mixing in non-quasi-static time-periodic cavity flows

Patrick D. Anderson *, Oleksiy S. Galaktionov, Gerrit W.M. Peters, Frans N. van de Vosse, Han E.H. Meijer

Materials Technology, Dutch Polymer Institute, Eindhoven University of Technology, P.O. Box 513, 5600 MB Eindhoven, The Netherlands

Received 30 November 1998; accepted 15 October 1999

Abstract

Fluid mixing in a two-dimensional square cavity with a time-periodic pulsating lid velocity is studied. A spectral element technique for spatial discretization is combined with a continuous projection scheme for temporal discretization to obtain a numerical representation of the non-quasi-static velocity field in the cavity. It is well known that mixing in a cavity with a steady lid velocity results in linear mixing of fluid inside the cavity. Here, it is shown that superposition of a pulsating component on the steady lid velocity can lead to chaotic mixing in the core of the cavity. An extra steady motion of the opposite cavity wall, resulting in a small perturbation to the original flow, causes the chaotically mixed region to be spread over almost the whole cavity. Poincaré and periodic point analysis reveal the main characteristics for these transient time-periodic flows, and elucidate the details and properties of the chaotic mixing in these flows.

Keywords: Chaotic mixing; Cavity flow; Periodic points; Poincaré mapping

Notation

$d(\mathbf{X})$	displacement of the particle $\mathbf{X}$ after one period
$\mathbf{F}_\mathbf{X}$	displacement gradient matrix
$l(t)$	circumference of the blob at time t
l_0	initial circumference of the blob
L	cavity length
p	pressure
P	amplitude of the oscillating top wall
$\mathscr{P}$	periodic point
$\mathscr{G}$	grid of points
q	pressure related quantity
Re	Reynolds number defines as $Re = \rho UL/\mu$
St	Strouhal number defined as $St = 2\pi L/(UT)$
s	local time within a time step
$s(\mathbf{X})$	local stretching near the particle $\mathbf{X}$ during one period
t	time
T	period of the oscillating top wall
Δt	time step
U	characteristic velocity
$\mathbf{u}$	dimensionless velocity field
U_{bot}	dimensionless velocity of the bottom wall
U_{top}	dimensionless velocity of the top wall
u	horizontal dimensionless velocity component
v	vertical dimensionless velocity component
$\mathbf{x}$	current position of the particle
$\mathbf{X}$	initial position of the particle
X	dimensionless horizontal coordinate
Y	dimensionless vertical coordinate
Greeks	
λ	eigenvalue
μ	dynamic viscosity
ρ	density
Ω	flow domain
Φ_t	mapping corresponding to the flow till time t
σ	eigenvalue spectrum of $\mathbf{F}_\mathbf{X}$

1. Introduction

Time-periodic oscillations of non-quasi-static flows can yield chaotic mixing, which itself leads to improvement of mass and heat transfer properties, see for example Baird et al. (1996), Hewgill et al. (1993), Howes et al. (1991), Mackley et al. (1996, 1990) and Nishimura and Kojima (1995). The effect of flow oscillations on mass transfer enhancement has been investigated for reciprocating plate columns and baffled tubes, see e.g. Hewgill et al. (1993), and Baird et al. (1996), while their effect on mixing and heat transfer was determined for different values of the Strouhal number, see Howes et al. (1991), and Mackley et al. (1996, 1990). These studies show that an oscillatory fluid motion can lead to chaotic mixing but an analysis of the chaos in the flow has not yet been presented. The objective of this study is to analyse the details of the characteristics of this chaos by applying computational methods. For this goal, the cavity flow with an oscillating, time-periodic lid velocity is studied, using well-known methods as contour

* Corresponding author. Tel.: +31-40-2472851; fax: +31-40-2447355.
E-mail address: patricka@wfw.wtb.tue.nl (P.D. Anderson).

0142-727X/00/$ - see front matter
PII: S0142-727X(99)00073-9

tracking, periodic point analysis and Poincaré mappings (see Ottino (1989)).

Numerous experimental and computational studies have demonstrated that mixing in cavity flows can be enhanced by time-periodic motion of bottom and top wall, see e.g. Anderson et al. (1999), Aref (1984), Chien et al. (1986), Leong and Ottino (1989), Liu et al. (1994). Generally, the flows are quasi-static, the mixing fluids considered are highly viscous and, consequently inertia forces are negligible. The flow is then determined by the Stokes equations and the dynamical tools, like periodic point analysis, used to analyse the mixing characteristics often rely on symmetry in the velocity field, i.e. symmetry of the streamlines. In the present study chaotic mixing is analysed for flows determined by the full Navier–Stokes equations, where stationary and non-stationary inertia forces cannot be neglected and where, consequently, the symmetry is broken. Although it is commonly believed (see e.g Jana et al. (1994)) that for such a flow without evident symmetry, periodic point analysis and Poincaré sections are less practical, these analysis methods can efficiently be applied, as it is shown in this study.

2. Mathematical formulations

The unsteady two-dimensional laminar motion of an incompressible Newtonian fluid within a square cavity is considered (see Fig. 1), where the non-quasi-static mixing flow is induced by a time-periodic motion of the upper wall. The motion of the incompressible fluid is described by the Navier–Stokes equations, which read in dimensionless form:

$$St\,\frac{\partial \mathbf{u}}{\partial t}+(\mathbf{u}\cdot\nabla)\mathbf{u}=-\nabla p+\frac{1}{Re}\nabla^2\mathbf{u}, \tag{1}$$

$$\nabla\cdot\mathbf{u}=0, \tag{2}$$

where $Re=\rho UL/\mu$ is the Reynolds number and $St=2\pi L/UT$ is the Strouhal number. The dynamic viscosity is denoted by μ, density by ρ, U and L are, respectively, the characteristic velocity and length. T is the duration of a period in time. The boundary conditions for $\mathbf{u}=(u,v)^{\mathrm{T}}$ read:

$$\begin{cases} u=U_{\mathrm{top}}=1+P\sin(\frac{2\pi t}{T}) & v=0 \quad \text{top wall},\\ u=0 & v=0 \quad \text{side and bottom walls}. \end{cases} \tag{3}$$

Since for $Re>0$ no analytical solutions are available for the velocity field in a cavity with oscillatory lid velocity, numerical techniques need to be applied. The Navier–Stokes equations are here discretized in time using an approximate projection method. This semi-implicit scheme is proposed by Timmermans et al. (1996) and proceeds as follows. The non-linear convection part is treated by means of an operator-integrating splitting approach (see Maday et al., 1990), and the remaining "Stokes equation" is discretized by means of a second-order backward difference scheme:

$$St\,\frac{3\mathbf{u}^{n+1}-4\tilde{\mathbf{u}}^{n}+\tilde{\mathbf{u}}^{n-1}}{2\Delta t}=-\nabla p^{n+1}+\frac{1}{Re}\nabla^2\mathbf{u}^{n+1},\qquad \nabla\cdot\mathbf{u}^{n+1}=0. \tag{4}$$

Here, the quantities marked by tildes are the corresponding quantities at level $n-i$ $(i=0,1)$, convected according to the following equation:

$$St\,\frac{\partial\tilde{\mathbf{u}}^{n-i}(s)}{\partial s}=(\tilde{\mathbf{u}}^{n-i}\cdot\nabla)\tilde{\mathbf{u}}^{n-i},\quad 0\leqslant s\leqslant(i+1)\Delta t,\ \ i=0,1,\qquad \tilde{\mathbf{u}}^{n-i}(0)=\mathbf{u}^{n-i}. \tag{5}$$

Eq. (5) is discretized by a fourth-order Runge–Kutta scheme. The projection scheme now proceeds as follows:

- A predictor $\mathbf{u}_p^{n+1}$ for the velocity at level $n+1$ is calculated using the pressure at level n as a predictor for the pressure at level $n+1$:

$$St\,\frac{3\mathbf{u}_p^{n+1}-4\tilde{\mathbf{u}}^{n}+\tilde{\mathbf{u}}^{n-1}}{2\Delta t}=-\nabla p^{n}+\frac{1}{Re}\nabla^2\mathbf{u}_p^{n+1} \tag{6}$$

  and imposing the velocity boundary conditions of level $n+1$ on it.
- By subtracting (6) from (4) and applying the divergence operator to both sides of the result, an equation for $q^{n+1}=p^{n+1}-p^{n}+(1/Re)\nabla\cdot\mathbf{u}_p^{n+1}$ is obtained. It reads:

$$\nabla^2 q^{n+1}=St\,\frac{3\nabla\cdot\mathbf{u}_p^{n+1}}{2\Delta t}. \tag{7}$$

  As it is justified by Timmermans et al. (1996), a homogeneous Neumann boundary condition for q^{n+1} can be used.
- Finally the velocity and pressure at level $n+1$ (the correctors) are calculated according to:

$$\mathbf{u}^{n+1}=\mathbf{u}_p^{n+1}-\frac{2\Delta t\nabla q^{n+1}}{3St},\qquad p^{n+1}=p^{n}+q^{n+1}-\frac{1}{Re}\nabla\cdot\mathbf{u}_p^{n+1}. \tag{8}$$

The Helmholtz equations (6) and Poisson equation (7) are discretized in space applying a spectral element discretization

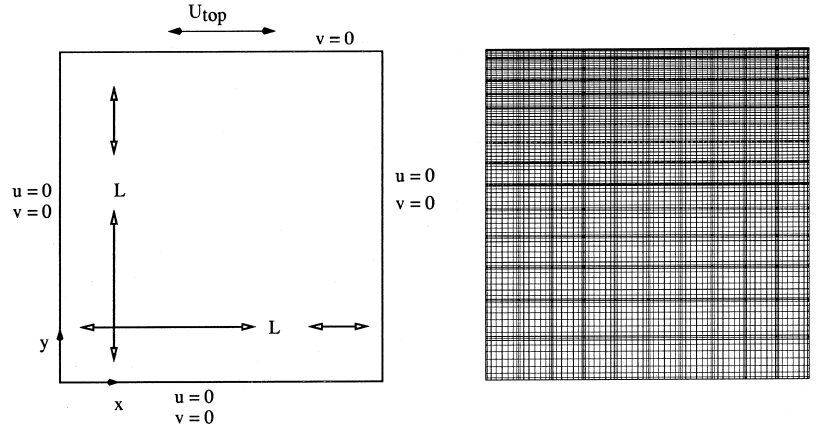

Fig. 1. Left: Geometry of the cavity with time-periodic oscillatory lid velocity. Right: Finite element representation of the spectral element mesh. It consists of 10×15 spectral elements each of order eight yielding totally 9801 non-uniformly distributed nodal points.

(see Maday and Patera, 1989) resulting in positive definite linear systems for $\mathbf{u}_p^{n+1}$ and q^{n+1}. They are suitable to be solved by a conjugate gradients algorithm, and a finite element preconditioner has been proven to be efficient in sense of both memory usage and CPU-time, see Anderson and van de Vosse (1998). Studies by Timmermans (1994) have shown that application of this projection in combination with spectral elements yields small numerical diffusion and dissipation errors, a characteristic for spectral methods in general, see Patera (1984).

In previous studies on this flow it was concluded that the effect of the Reynolds number is limited with respect to the mixing process, see e.g. Takasaki et al. (1993), who examined the flow for $50 \leqslant Re \leqslant 500$. Therefore in our study the Reynolds number Re is fixed and set to 50, while the Strouhal number St is varied within the range $0.5 \leqslant St \leqslant 12$, and the amplitude P of the oscillations takes the values $0, 0.5,$ and 1.5. For $P = 0$ the lid velocity is constant, for $P = 0.5$ the lid velocity oscillates, but remains uni-directional and in the last case $P = 1.5$ the lid velocity also changes its sign.

The initial velocity and pressure in the cavity are set to zero and for the range of parameters investigated, after approximately 10 periods the time-periodic boundary conditions induce a time-periodic flow with the same period T. This is certainly not trivial since the momentum equation is non-linear. The flow could have been non-periodical or periodic with a different frequency. The maximum norm difference between two velocity fields at times differing by exactly one period of excitation is computed, and, for the simulations presented in this study, it holds that

$$\exists_{T_1}\ \forall_{t>T_1} \qquad \|\mathbf{u}(\mathbf{x}, t+T) - \mathbf{u}(\mathbf{x}, t)\|_\infty \leqslant P \times 10^{-5}, \tag{9}$$

where $\|\cdot\|_\infty$ denotes the maximum norm. Consequently, all solutions presented are time-periodic, and in the mixing analysis the influence of the initial conditions on velocity has disappeared.

For all cavity flows considered in this paper, typically 300 time steps were used within one period in order to obtain numerical stability for the convection equation (5). The spectral element mesh which was used is depicted in Fig. 1. The present study does not intend to give a detailed analysis of the velocity field in a cavity with an oscillating lid (see Nishimura and Kunitsuga (1997) for an extensive analysis on vortex strength for different Strouhal numbers), but aims to give an analysis of the chaotic mixing behaviour of this flow. For amplitudes larger than one, like the case $P = 1.5$, the lid velocity becomes negative, the clockwise rotation still persists and a counterclockwise recirculation is generated just below the top wall. The centre of the clockwise rotating vortex mainly oscillates in the vertical direction during the time period motion of the lid.

3. Chaotic fluid mixing

3.1. Tracking of fluid elements

The study of fluid mixing starts with the analysis of the motion of fluid elements by the imposed velocity field, thus by investigating the dynamical system:

$$St\frac{\mathrm{d}\mathbf{x}}{\mathrm{d}t} = \mathbf{u}(\mathbf{x}, t), \tag{10}$$

where $\mathbf{u}(\mathbf{x}, t)$ is assumed to be known. Note that Eq. (10) is made dimensionless similar to the momentum equation (2). The integration of (10) with the initial condition $\mathbf{x} = \mathbf{X}$ at $t = 0$ for a time length T gives the position of particle $\mathbf{x}$ at $t = T$. The flow can be represented by

$$\mathbf{x} = \Phi_t(\mathbf{X}), \qquad \mathbf{X} = \Phi_{t=0}(\mathbf{X}), \tag{11}$$

mapping particle $\mathbf{X}$ to $\mathbf{x}$ after a time t. It should be noted that there is no diffusion of particles, and that the particles are passive markers within the fluid. This viewpoint is purely kinematic and all the complexities in solving the dynamical system are associated with obtaining $\mathbf{u}(\mathbf{x}, t)$.

From the spectral element discretization, the velocity is only known in a limited number of grid points and for a limited number of time steps within a period. Tracking material points in a flow requires the knowledge of the velocity of the fluid in any arbitrary point in the flow domain at any moment. Therefore, interpolation of the velocity field is necessary. The accuracy of the interpolation is always limited to the accuracy of the discretized data. To ensure that the interpolation error is of the same order as the approximation error (of the discretized data) a consistent interpolation scheme based on the same polynomial basis functions which are used within the numerical discretization is necessary (see for example the work of Souvaliotis et al. (1995) on the effects of approximation and interpolation errors). Between time levels a linear interpolation is used to obtain the velocity field at an intermediate time level, also the same as the discretization order. The dynamical system (10) is numerically integrated using an adaptive Runge–Kutta scheme (see Press et al. (1992)), and errors in the trajectories of particles are mainly imposed by discretization errors of the numerical velocity field. The tracking of particles is highly parallelizable and, in this study, is performed on a cluster of 60 Pentium Pro© personal computers. For results on the parallel efficiency the reader is referred to Galaktionov et al. (1997).

3.2. Chaotic advection

To quantify the mixing efficiency, the time evolution of a strip placed in the square cavity ($L = 1$) is studied. Results are presented in Fig. 2. An adaptive front tracking technique as presented in Galaktionov et al. (2000) and also applied in Anderson et al. (1999) is used to follow the material strip (instead of designating the strip by a number of uniformly distributed material points, the boundary of the strip is tracked, where, based on a required quality of the description of the contour, points are adaptively added or removed during tracking).

For the amplitudes $P = 0$, 0.5, and 1.5, numerically computed velocity fields are applied to study the influence of P on mixing using a fixed Strouhal number. The case $P = 0$ is used as a reference where no oscillations are present. For one set of parameters, $P = 0.5$ and $St = 4.2$, the characteristics of mixing are studied in more detail using a periodic point analysis.

The chaotic advection of the material strip placed in the cavity is studied for each of the three amplitudes. The strip is placed vertically in the cavity, and has the dimensions $0.495L \leqslant X \leqslant 0.505L$, $0.1L \leqslant Y \leqslant 0.9L$. For amplitude $P = 0$ (steady motion) only a linear increase in interfacial area of the strip is observed, see Fig. 2 and Table 1. In Nishimura and Kunitsuga (1997) the line $X = 0.5L$, $0.1L \leqslant Y \leqslant 0.9L$ was tracked and their results for $t = 8$ show a good agreement with the results presented in Fig. 2. Here, a strip is tracked instead of a line in order to visualize areas of bad mixing, indicated by low local stretching. For $P = 0.5$ and $P = 1.5$ the material strip is not constrained to follow steady streamlines (in contrast to $P = 0$) and is much more effectively distributed over a large part of the flow domain. The stretching and folding process of fluid elements, strongly enhancing the fluid mixing, clearly can be observed in Fig. 2. The generation of interfacial

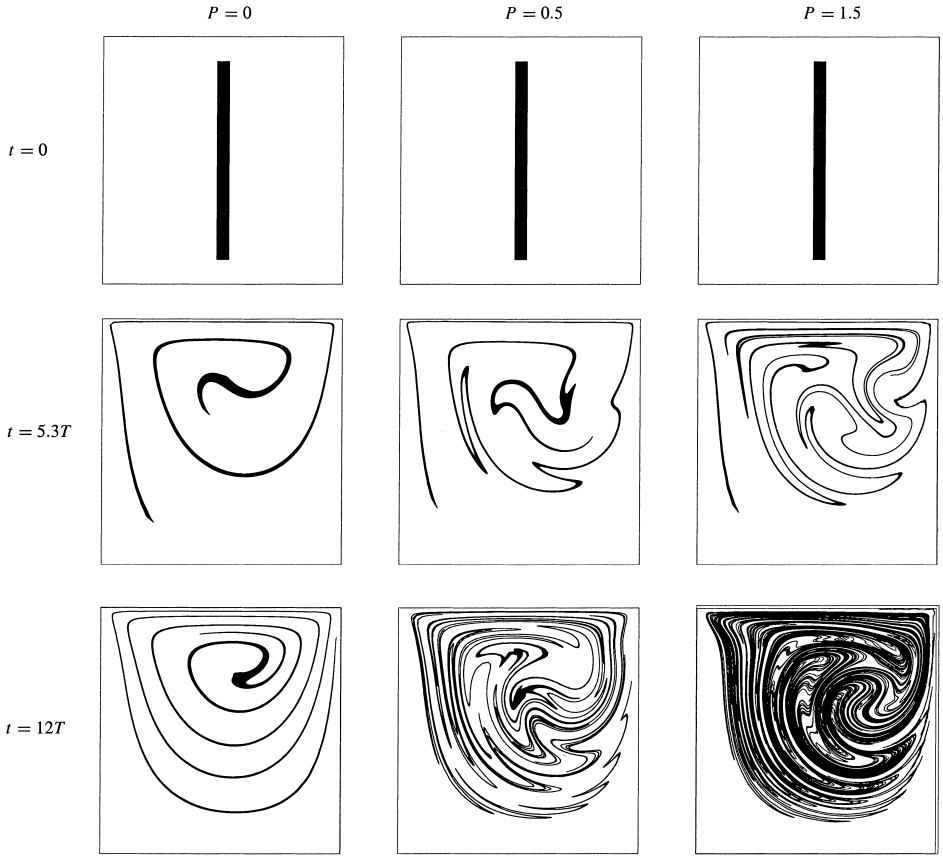

Fig. 2. Deformation of the material strips in the top row; left column strips are the deformation for $P = 0$; middle column strips are the deformation for $P = 0.5$, and the pictures in the right column are for $P = 1.5$. The middle row figures display the advection after $t = 8 = 5.3T$, and the lower figures show the deformation at $t = 12T$. Here, $T = 1.5$, resulting in a Strouhal number $St = 4.2$.

Table 1
The influence of the amplitude P on the circumference of the advected strips shown in Fig. 2[a]

	$t = 0$	$t = 3T$	$t = 6T$	$t = 9T$	$t = 12T$
$P = 0$	1.7	5.8	9.7	14.7	17.0
$P = 0.5$	1.7	5.6	13.0	30.0	57.0
$P = 1.5$	1.7	8.7	39.7	162	608

[a] The exponential increase in interfacial area is clear for $P = 0.5$ and $P = 1.5$. The results are for $T = 1.5$, resulting in a Strouhal number $St = 4.2$.

area is shown in Table 1. The table shows that for a P larger than zero, an exponential increase of interfacial area, and therefore efficient mixing, can occur. The results at the time $t = 8 \approx 5.3T$ are shown to allow for a comparison with Nishimura and Kunitsuga (1997). The computed area conservation of the advected strips is within 1% over 12 periods, indicating accurate tracking.

4. Mixing analysis: periodic points and Poincaré maps

Advection of material fluid elements, as discussed above, provides insight into the rate of mixing. An asymptotic picture of the mixture follows from a Poincaré map, which is less computationally expensive to obtain. For $P = 0$ the Poincaré section, Fig. 3, reveals the streamlines of the flow, since there is only a steady movement of the upper wall. The Poincaré sections for the flows with parameters $P = 0.5$ or $P = 1.5$, and $St = 4.2$ are also shown in Fig. 3. An initial grid of 100 markers, uniformly distributed over the flow domain, is tracked for 500 periods to create the asymptotic pictures of the mixture.

The Poincaré section for $P = 0.5$ shows that the particles are reasonably well spread over a large part of the cavity, but that there are, apart from the region close to the stationary walls, four poor-mixing regions located in the core of this flow. The presence of regions of regular motion in the core is studied in detail by means of a periodic point analysis.

The main characteristics of chaotic mixing can be determined by the location and nature of the periodic points. By definition, periodic points are points which return to their original position after one or more periods of flow. Using the definition of the mapping in Eq. (11), a periodic point $\mathscr{P}$ of order n is defined as:

$$\Phi_{nT}(\mathscr{P}) = \mathscr{P}, \tag{12}$$

$$\Phi_{mT}(\mathscr{P}) \neq \mathscr{P} \quad \text{for } m < n, \tag{13}$$

where T is again the duration of one period of motion. Periodic points are classified according to the nature of the

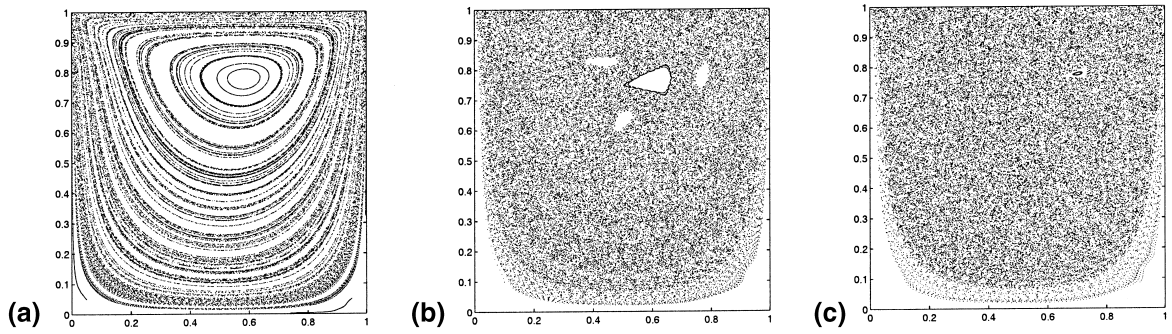

Fig. 3. Poincaré section after 500 periods: (a) $P = 0$; (b) $P = 0.5$, $St = 4.2$; (c) $P = 1.5$, $St = 4.2$.

deformation in their neighbourhood. Elliptic (stable) periodic points are at the centre of non-mixing rotating regions, called islands, while hyperbolic (unstable) periodic points are centres of stretching in the flow.

Determination of periodic points in this type of flows is not as straightforward as for systems where stationary and unstationary inertia forces are absent. For those flows it is often possible to use symmetry of the streamlines to simplify the detection of periodic points. For the mixing flows studied here such techniques cannot be applied, and a more general method, as presented by Anderson et al. (1999), is used to find periodic points.

A grid $\mathscr{G}$ of markers (100×100) is uniformly placed in the cavity (not touching the cavity walls) and tracked for one period of motion. The displacement $d(\mathbf{X})$ and stretching $s(\mathbf{X})$ are computed for each marker after one period, using the definitions

$$d(\mathbf{X}) = \|\mathbf{X} - \Phi_T(\mathbf{X})\|_2, \tag{14}$$

and

$$s(\mathbf{X}) = \max_{\lambda \in \sigma(\mathbf{F_X})} |\lambda|, \tag{15}$$

where $\sigma(\mathbf{F_X})$ is the eigenvalue spectrum of $\mathbf{F_X}$, the displacement gradient, defined as $\mathbf{F_X} = (\nabla_{\mathbf{X}} \Phi_T(\mathbf{X}))^{\mathrm{T}}$.

The results are presented in Fig. 4. In the core of the cavity a region of low displacement is detected, and a further refinement of the grid $\mathscr{G}$ indicates a root of $d(\mathbf{X}) = 0$, and consequently the presence of a first-order periodic point. Since there is no stretching around the first-order periodic point, it is concluded that the nature of this point is elliptic. If the displacement and stretching are now computed over three periods in a zoomed region in the cavity, much more details are revealed, see Fig. 5, and seven regions of low displacement (around roots of $d(\mathbf{X}) = 0$) are observed. The central of the seven regions, which was earlier classified as a first-order elliptic periodic point, obviously also has a low displacement after three periods of motion. The nature of the six third-order periodic points is revealed by the stretching picture after three periods, presented in Fig. 5(b). The three points nearest to the first-order point are located in a low-stretching region, while the other three are in a high-stretching zone. The first three are obviously elliptic points (which was also clear from the Poincaré section), and the three other third-order periodic points are of hyperbolic type. The large island in the middle of Fig. 3(b), is thus located around a first-order elliptic periodic point, while the three other smaller islands are located around third-order elliptic periodic points, as follows from numerical analysis of the flow.

Kolmogorov–Arnold–Moser (KAM) boundaries separate regions of regular and chaotic flow, see Ottino (1989). If a surface coinciding with KAM boundary at $t = 0$ is placed around the first-order elliptic point it will return to its original position after one period. If such surfaces are placed around

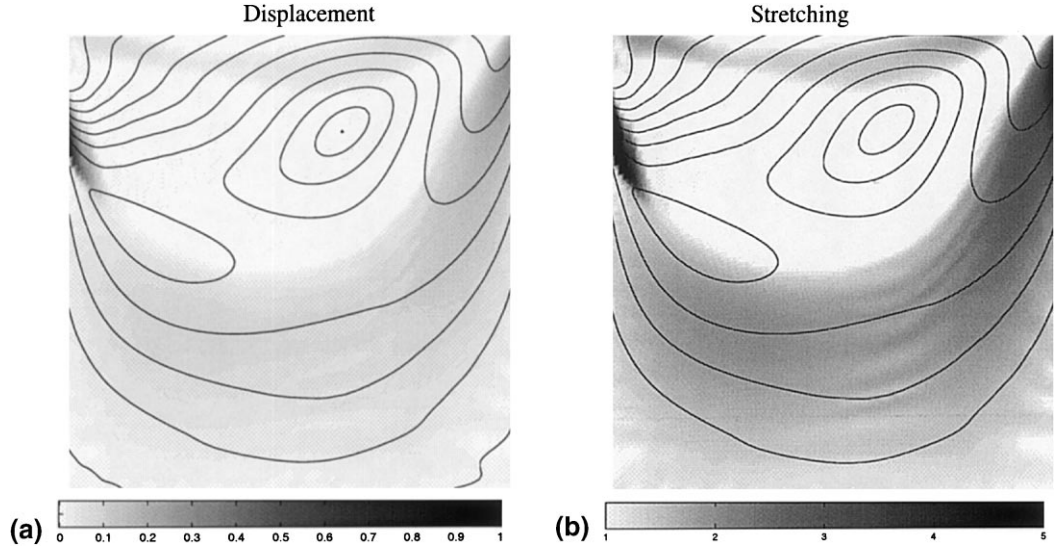

Fig. 4. Displacement (a) and stretching (b) after one period; $St = 4.2$ and $P = 0.5$. For the stretching plot a threshold maximum value 5 is used, where the maximum stretching value equals 14.4.

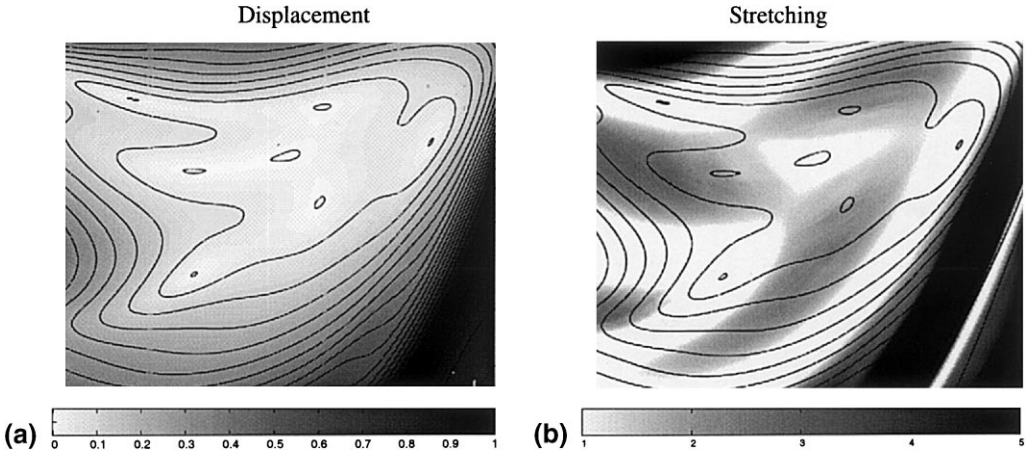

Fig. 5. Displacement (a) and stretching (b) after three periods for a *zoomed* region around the set of islands ($0.4L < X < 0.85L$, $0.5L < Y < 0.95L$); $St = 4.2$ and $P = 0.5$. The maximum stretching value after three periods equals 65.5.

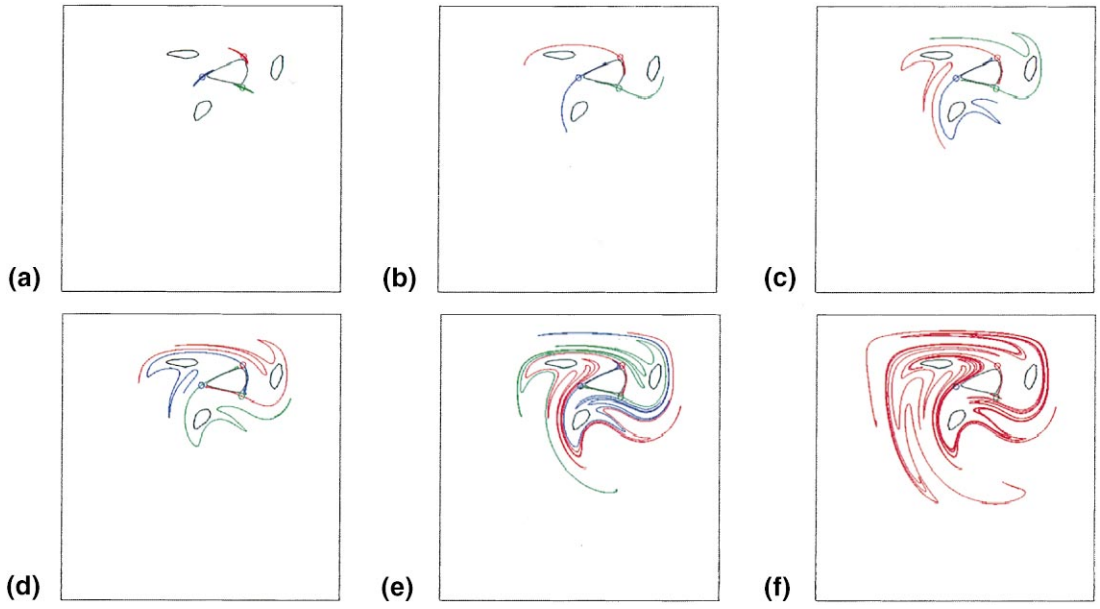

Fig. 6. Advection of blobs placed around third-order hyperbolic points. Figures (a)–(c) show advection after 6, 12 and 18 periods. Plot (d) shows the advection after 19 periods and (e) after 24 periods. Finally in figure (f) the advection of a single blob placed around the upper hyperbolic point is shown after 30 periods. The Strouhal number is equal to 4.2 and the amplitude P equals 0.5.

the third-order elliptic points and tracked for one period, then they undergo a cyclic permutation with each other. Such a permutation is repeated each new period.

In Fig. 6 the advection of blobs (with an original diameter $h = 0.05L$, where L is the width of the cavity) around the third-order hyperbolic points is presented. After each multiple of three periods the blob intersects with its original position. During the first 12 periods the deformation of the blobs only appears to be minor, but during the next 12 periods the effect of exponentially stretching (and consequent folding around the elliptic points) becomes clear. In Fig. 6(c) the location of the blobs after 18 periods is depicted. One period later, Fig. 6(d), the location of the blobs is shifted, and they are located around the next hyperbolic periodic point. The deformation of a single blob after 30 periods is presented in Fig. 6(f). The sequence of pictures show that the stretching and folding takes place between the islands, where the islands appear to "attract" folds.

In Fig. 7 a zoomed region from Fig. 6(f) is displayed. This figure shows how the unstable manifold of one hyperbolic cycle is connected with the stable manifold of another hyperbolic cycle. This connection, called a heteroclinic connection, is here shown between two third-order hyperbolic points. Obviously, two more heteroclinic connections are present in this flow.

One of the most simple measures to quantify the degree of mixing is the stretching of a material blob in the flow. Such a measure was used in, for example Ottino (1989), and Nishimura and Kunitsuga (1997). The line (boundary) stretching, $l(t)/l_0$, for the blobs of Fig. 6 placed around the upper hyperbolic point is shown in Table 2, and the blob circumference exponentially grows as $l(t) \approx l_0 e^{0.23t/T}$. It should be noted that if a non-adaptive technique is applied to track the contours of the blobs, misleading results may be obtained, since in that case only during the first periods, mixing is exponential, but

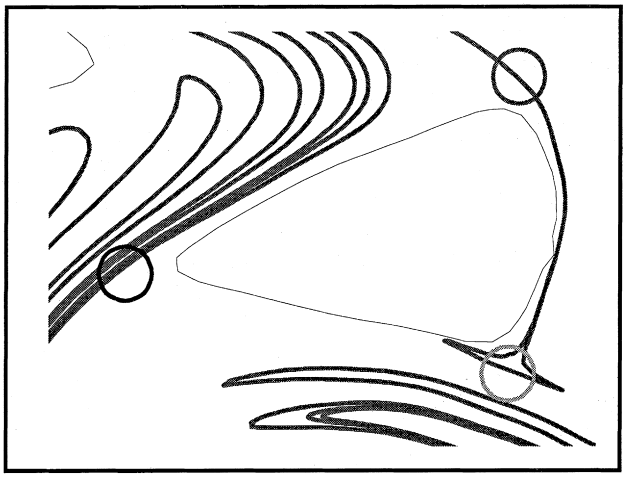

Fig. 7. Here a region around the hyperbolic points in Fig. 6(f) is enlarged. The red blob is stretched along its unstable manifold and intersects with the stable manifold of another hyperbolic point (heteroclinic connection). As it enters the stable manifold it is stretched along the unstable manifold.

later it becomes only linear. Such a *wrong* conclusion is mainly the result of the difficulties associated with tracking contours in chaotic flows; when no adaptive contour tracking method is used, a stretched and folded contour part which is not resolved may grow between two adjacent contour points.

For the flow with amplitude $P = 1.5$ a similar analysis has been performed. The Poincaré section for this mixing flow is presented in Fig. 3(b). Compared to the situation $P = 0.5$, here the stretching rates are much higher (maximum stretching value of 17.7 after one period and 117.2 after three periods), but a similar set of periodic points is found located much closer to each other.

In addition to the amplitude, the Strouhal number is also an important parameter that controls the flow and mixing characteristics. If the Strouhal number for a fixed amplitude P, say $P = 1.5$, is too large or too small, the unstable (hyperbolic) periodic points will disappear and as a result the mixing quality will decrease. If the Strouhal number is large then the time period of the oscillations is small, having a minor effect on the stretching and folding. For a small Strouhal number the flow resembles the linear mixing steady flow. For two extreme Strouhal numbers, $St \approx 0.6 (T = 10)$ and $St \approx 13 (T = 0.5)$, a similar periodic point analysis was performed. For these flows no hyperbolic points, the source for stretching and folding, (up to fourth order) could be detected. This explains the advection results presented in Nishimura and Kunitsuga (1997). For the steady flow ($P = 0$) only a single stationary point is located in the centre of the main vortex, explaining the poor mixing for this parameter. Nishimura and Kunitsuga (1997) also considered three different aspect ratios and they calculated the line stretching for different Strouhal numbers. For these aspect ratios they found that the change of aspect ratios will probably lead to poorer mixing. Based on the maximum line stretch they concluded that there is an optimal Strouhal number that yields the "best" mixing for each aspect ratio. In their research, optimal mixing occurs for the original aspect ratio (square cavity) with a Strouhal number approximately equal to 5. Some caution should be used with respect to this conclusion, since high stretching itself does not necessarily imply good mixing. It is possible that fluid elements undergo exponential stretching, but they remain in a limited part of the flow domain. Proper use of mixing measures is discussed by Tucker (1991) in detail.

The fluid element advection results in Fig. 6, and the Poincaré sections in Fig. 3 show that although chaotic mixing can be present in the square cavity with an oscillating lid-velocity, mixing in the bottom of the cavity remains poor. In the next section some possible improvements of the original system are proposed to increase the extent of mixing.

5. Improving mixing performance

The previous sections showed that an oscillating lid-velocity can produce chaotic mixing. In the upper half of the square cavity the mixing is chaotic, while the quality of mixing remains poor near the bottom and side walls of the cavity. Several measures can be considered that could yield a more uniform mixture. Examples include changing the geometry introducing curved geometries, or changing in the aspect ratio of the cavity, or a change in the Strouhal number, and, finally, by introducing a more complex boundary condition (for example also a motion of the bottom cavity wall). Here the influence of a steady movement of the bottom wall on the mixing ability is investigated. This causes the stagnation regions in the bottom of the cavity to disappear, and allows the fluid to reach the chaotic region.

For one set of parameters, $P = 1.5$, $St = 4.2$, and four bottom velocities the velocity fields during a period are computed ($U_{\text{bot}} = \pm 1$, $U_{\text{bot}} = \pm 0.1$). Similar to the original situation with a fixed bottom wall, again a time-periodic velocity field is induced by the time-periodic boundary condition at the top wall, and compared to $U_{\text{bot}} = 0$, the corner cells are absent in the bottom half of the cavity where now velocity gradients are present. The main vortex is still present and its centre moves in vertical direction up and down during a period. Again, a separation zone is visible as a response to the sign change of the velocity of the upper wall.

Computational methods are once more applied to gain insight in the chaotic behaviour of the flow. First, Poincaré sections are computed and the results are presented in Fig. 8. For $U_{\text{bot}} = -1$ a structure with seven islands is revealed. The two large islands at approximately the vertical centre line are surrounding first-order elliptic points. The five other islands are around fifth-order elliptic points, a situation similar to Fig. 3(a), which has third-order periodic points. A first-order periodic points analysis, see Fig. 9, shows that between the first-order elliptic points a first-order hyperbolic point, previously not present, is located. Stretching and displacement results after five periods reveal five additional periodic points of hyperbolic type located between the high-order islands.

Table 2
Increase in interfacial length during advection of material blobs, orginally placed around third-order hyperbolic periodic points[a]

	$t = 0$	$t = 3T$	$t = 6T$	$t = 12T$	$t = 18T$	$t = 24T$	$t = 30T$
red blob	0.0627	0.0911	0.1895	0.8928	2.6617	10.734	64.159
green blob	0.0627	0.0867	0.1577	0.5890	2.2888	6.0233	47.395
blue blob	0.0627	0.0966	0.1884	0.6474	1.7429	7.442	35.889

[a] The results are for $T = 1.5$, resulting in a Strouhal number $St = 4.2$, and the amplitude of the oscillations equal 0.5.

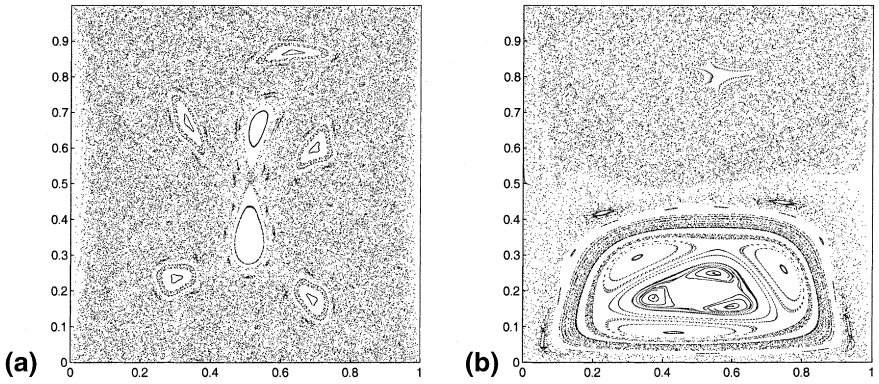

Fig. 8. Poincaré section after 500 periods. In figure (a) results are shown for $P = 1.5$ and $St = 4.2$ with a negative steady movement of the bottom wall, i.e. $U_{bot} = -1$. In (b) for the flow conditions but now with a positive movement, i.e. $U_{bot} = 1$.

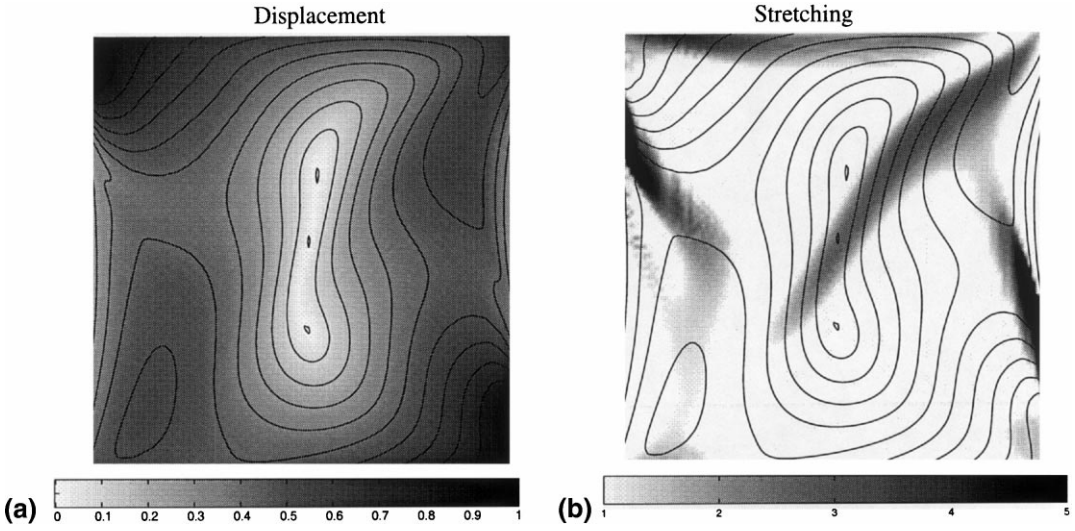

Fig. 9. Displacement (a) and stretching (b) after one period; $St = 4.2$ and $P = 1.5$. The bottom wall has a steady velocity of $U_{bot} = -1$. The maximum stretching after one period equals 17.8.

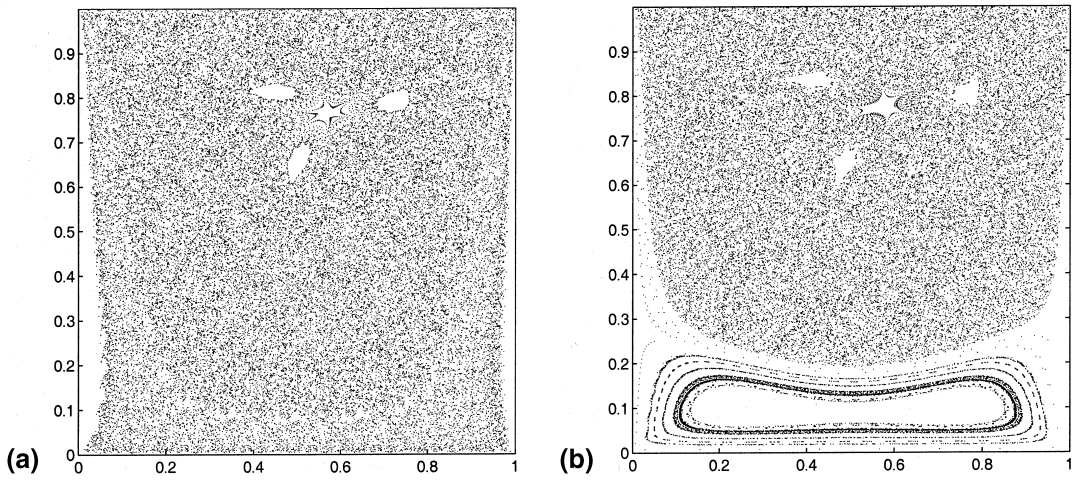

Fig. 10. Poincaré section after 500 periods. In figure (a) results are shown for $P = 1.5$ and $St = 4.2$ with a small steady movement of the bottom wall in negative x direction, i.e. $U_{bot} = -0.1$. In (b) for similar flow conditions but now with a movement in positive x direction.

Although the mixing in the lower half of the cavity has improved, the global mixing quality seems not to be improved drastically in terms of the total area of the islands.

If the bottom wall moves in the positive x direction, $U_{bot} = 1$, the mixing quality decreases drastically. The Poincaré section, Fig. 8(b), reveals a large recirculation region in

the lower half of the cavity. Inside this separated zone some remarkable structures are present, but this structure is not further investigated because of lack of interaction with the remainder of the cavity.

In Fig. 10(a), results are shown for $P = 1.5$ and $St = 4.2$ with a small steady movement of the bottom wall in the negative x direction, $U_{bot} = -0.1$. In Fig. 10(b) we see results for the same flow conditions but now with a movement in positive x direction. Also here the direction of the bottom wall movement has a large influence on the mixing in the cavity. Even if the bottom wall moves with a velocity as low as $U_{bot} = 0.1$, a strong negative effect on mixing is observed. A separated rotation region is generated where the fluid elements are only stretched linearly, and where there is no interaction with the core of the flow.

6. Conclusions and discussion

Fluid mixing in a prototype cavity flow with an oscillating lid velocity was examined for a Navier–Stokes flow. For these inertia-dominated flows, the symmetry of the flow is destroyed and a periodic point analysis is more difficult. Computational methods have been developed and applied for the analysis of these type of flows, resulting in a set of general tools. The major conclusions are:

- Superimposing an unsteady component of the lid velocity on the steady flow results in an exponential increase of interfacial length, due to stretching and folding of fluid volumes in the flow.
- A time-periodic boundary condition in a non-linear flow can lead asymptotically to a time-periodic flow.
- Computational tools like periodic point analysis and Poincaré sections can be applied for non-quasi-static, time-periodic flows.
- For the cavity flow studied here, movement of the bottom wall will only positively affect the mixing if it is a perturbation in the opposite direction with respect to the upper wall motion. Otherwise, the effect can be a large decrease in the mixing quality, and, therefore, also in the mass and heat transfer capabilities.

The methods developed are general and can be applied to other non-quasi-static mixing problems, for example when the non-linearity results from the rheological properties of the fluid.

The presence of unstationary inertia forces in the prototype cavity flow with an oscillating lid velocity allowed an exponential increase in interfacial area. The corresponding oscillation frequency has a significant effect on mass transfer capabilities in the cavity flow. As long as the Strouhal number is of the order of 5 compared to the steady motion of the wall, effective mixing results. For Strouhal numbers of order of either 1 or 10, the influence of the oscillations is less effective and mixing will be poorer. The effect of the amplitude of the oscillations, for a fixed Reynolds number, can be significant. It was found here that, if the amplitude is of equal order compared to the steady motion, chaotic advection of fluid elements is possible. The results indicate that in the range of investigated situations ($P = 0$, 0.5, and 1.5) a larger amplitude of the oscillations, compared to the steady component, leads to more stretching and folding of the fluid, and thus to better mixing. A smaller amplitude can also lead to chaotic advection, but it is expected that the mixing efficiency will be lower.

Another phenomenon that was observed during the computations is that elliptic points, and their associated islands, actually promote mixing efficiency. Fluid elements which are close to hyperbolic periodic points are advected *around* the islands. The islands act as obstacles for the fluid, and the fluid folds around the islands. Clearly, KAM boundaries separate the regular and chaotic mixing zones, and within the KAM boundaries the mixing is regular and linear. However, if the flow parameters are modified such that the islands disappear, then the route to effective mixing also disappears. It is therefore more effective to let the fluid stretch and fold around the islands, and then after a number of periods, modify or adjust the protocol such that well-mixed fluid *exchanges* with the fluid in the islands. One might also consider adding some marbles or solid fillers into the initial mixture. These will lead to stretching and folding of fluid elements and can be easily removed after the mixing process is finished. Another possibility might be to change the geometry or to create a mixing protocol with oscillations superimposed on the steady flow, and let the amplitude and/or the frequency be a function of time.

Acknowledgements

The authors would like to acknowledge support by the Dutch Foundation of Technology (STW), grant No. EWT44.3453.

References

Anderson, P.D., Galaktionov, O.S., Peters, G.W.M., van de Vosse, F.N., Meijer, H.E.H., 1999. Analysis of mixing in three-dimensional time-periodic cavity flows. J. Fluid Mech. 386, 149–166.

Anderson, P.D., van de Vosse, F.N., 1998. A finite element preconditioner for Stokes problems with non-constant coefficients. Paper presented in Tel Aviv, Israel, June 1998. Proceedings of ICOSAHOM.

Aref, H., 1984. Stirring by chaotic advection. J. Fluid. Mech 143, 1–21.

Baird, M.H.I., Rama Roa, N.V., Stonestreet, P., 1996. Power dissipation and hold-up in a gassed reciprocating plate column. IChemE 74, 463–469.

Chien, W.L., Rising, H., Ottino, J.M., 1986. Laminar mixing and chaotic mixing in several cavity flows. J. Fluid. Mech. 170, 355–377.

Galaktionov, A.S., Anderson, P.D., Peters, G.W.M., 1997. Mixing simulations: tracking strongly deforming fluid volumes in 3D flows. In: Bubak, M., Dongarra, J., Wasniniewski, J. (Eds.), Recent advances in Parallel Virtual Machine and Message Passing Interface, volume 1332 of Lecture Notes in Computer Science. Springer, Berlin, pp. 463–469.

Galaktionov, A.S., Anderson, P.D., Peters, G.W.M., van de Vosse, F.N., 2000. An adaptive front tracking technique for three-dimensional transient flows. Int. J. Numer. Meth. Fluids 32, 201–213.

Hewgill, M.R., Mackley, M.R., Pandit, A.B., Pannu, S.S., 1993. Enhancement of gas–liquid mass transfer using oscillatory flow in baffled tubes. Chem. Eng. Sci. 48, 799–803.

Howes, T., Mackley, M.R., Roberts, E.P.L., 1991. The simulation of chaotic mixing and dispersion for periodic flows in baffled channels. Chem. Eng. Sci. 46, 1669–1677.

Jana, S.C., Tjahjadi, M., Ottino, J.M., 1994. Chaotic mixing of viscous fluids by periodic changes in geometry: Baffled cavity flow. AIChE Journal 40 (11), 1769–1781.

Leong, C.W., Ottino, J.M., 1989. Experiments on mixing due to chaotic advection in a cavity. J. Fluid. Mech. 209, 463–499.

Liu, M., Peskin, R.L., Muzzio, F.J., Leong, C.W., 1994. Structure of stretching field in chaotic cavity flows. Aiche 40 (8), 1273–1286.

Mackley, M.R., Stonestreet, P., Roberts, E.P.L., Ni, X., 1996. Residence time distribution enhancement in reactors using oscillatory flow. Trans IChemE 74, 541–545.

Mackley, M.R., Tweddle, G.M., Wyatt, I.D., 1990. Experimental heat transfer measurements for pulsatile flow in baffled tubes. Chem. Eng. Sci. 45, 1237–1242.

Maday, Y., Patera, A.T., Rønquist, E.M.R., 1990. An operator-integration-factor splitting method for time-dependent problems: application to incompressible fluid flow. J. Sci. Comp. 5, 263–292.

Maday, Y., Patera, A.T., 1989. Spectral element methods for the incompressible Navier–Stokes equations. In: Noor, A. (Ed.), State-of-the-Art surveys on computational mechanics. ASME, New York.

Nishimura, T., Kojima, N., 1995. Mass transfer enhancement in a symmetric sinusoidal wavy-walled channel for a pulsatile flow. Int. J. Heat Fluid Flow 38, 1719–1731.

Nishimura, T., Kunitsuga, K., 1997. Fluid mixing and mass transfer in two-dimensional cavities with time-periodic lid velocity. Int. J. Heat Fluid Flow 18, 497–506.

Ottino, J.M., 1989. The Kinematics of Mixing: Stretching, Chaos and Transport. Cambridge University Press, Cambdrige, MA.

Patera, A.T., 1984. A spectral element method for fluid dynamics: laminar flow in a channel expansion. J. Comp. Phys. 54, 468–488.

Press, W.H., Teukolsky, S.A., Vetterling, W.T., Flannerly, B.P., 1992. Numerical Recipes in Fortran, second ed. Cambridge University Press, Cambridge, MA.

Souvaliotis, A., Jana, S.C., Ottino, J.M., 1995. Potentialities and limitations of mixing simulations. AIChE J. 41 (7), 1605–1621.

Takasaki, S., Ogawara, K., Iida, S., 1993. A study on chaotic mixing in two-dimensional cavity flows. Nagare 12, 20–30.

Timmermans, L.J.P., 1994. Analysis of spectral element methods with application to incompressible flow. Ph.D. thesis, University of Technology, Eindhoven.

Timmermans, L.J.P., Minev, P.D., van de Vosse, F.N., 1996. An approximate projection scheme for incompressible flow using spectral elements. Int. J. Numer. Meth. Fluids 22, 673–688.

Tucker, C.L. Principles of mixing measurement. In: Chris Rauwendaal (Ed.), Mixing in Polymer Processing, Plastics Engineering. Marcel-Dekker, New York, 1991.